An Investigation of the Reduction in Tensile Strength and Fatigue Life of Pre-Corroded 7075-T6 Aluminum Alloy

B. Obert, K. Ngo, J. Hashemi, S. Ekwaro-Osire, and T.P. Sivam

(Submitted 14 September 1999; in revised form 8 March 2000)

In aging aircraft, the synergetic interaction between corrosion and fatigue has been shown to reduce the life expectancy of aluminum alloys. The objective of this study was to quantify the effects of corrosion, in terms of mass loss per unit area, on the static strength and fatigue life of 7075-T6 aluminum alloy. This was an experimental study in which test specimens were corroded in a laboratory environment. The corrosion process was accelerated by use of a corrosion cell. Test specimens were cut from flat sheets of aluminum and covered with masking material to restrict corrosion to a confined area. After testing, the fatigue life, ultimate tensile strength (UTS), and hardness of the specimens were observed to drop significantly with small amounts of corrosion. After the initial decrease, the UTS was observed to decrease linearly with increasing corrosion levels. The fatigue life of the specimens decreased in an inverse exponential fashion as mass loss per unit area increased. The hardness values of the corroded surfaces were also observed to drop. The topology of the pits and the related subsurface damage produced areas of high stress concentration resulting in the immediate reduction of UTS and fatigue life of the specimens. Subsurface corrosion damage was responsible for the reduction in hardness.

Keywords alloy 7075-T6, aluminum alloy, corrosion, fatigue, tensile strength

1. Introduction

Aging aircraft is currently an area of intense study and research. This surge in interest is due to the fact that in recent years many aircraft are approaching their design service life limit. Among the issues facing aging aircraft, corrosion in combination with fatigue is extremely undesirable. Corrosion can reduce the life of aircraft structures considerably. Corrosion on aircraft can be attributed to natural environmental factors such as humidity, rain, temperature, and salt water. Because of this impact on the life of aging aircraft, there is a need to understand, quantify, and monitor the corrosion process, particularly as it relates to structural fatigue life. Several techniques have recently been developed to detect various types of corrosion in aging aircraft. Most attractive to industry are nondestructive evaluation (NDE) techniques that reduce the down time of aircraft. This goal is achieved by minimizing disassembly at the time of scheduled maintenance checks. Green[10] presented a review of emerging technologies for the NDE of aging aircraft. The author, among others, also outlined *in situ* NDE techniques that could be used to continuously monitor aging aircraft structures. He noted that NDE techniques, due to their improving accuracy, will play a crucial role in the future. Recently, Crispim and da Silva[5] demonstrated that neutron radiographic images, produced with a suitable contrasting agent, have potential as an essential tool in the maintenance of aging aircraft in the future. A holistic approach on the maintenance of aging aircraft is presented by Feinberg *et al.*[7] In the latter paper, the authors proposed a flexible framework to administer reliability-guided maintenance corrosion programs. This framework was developed for the corrosion simulation of aging aircraft, which could be applied to the structural failure prediction with somedegree of certainty.

Among the different forms of corrosion, pitting is the form that is prevalent in aging aircraft, and is the main factor in most corrosion failures. Frankel[9] offered a detailed review on the factors that play a crucial role in the onset of pitting corrosion of metal. The author presents a concise outline of the phenomenology and stages of pitting. There have also been numerous studies on the impact of corrosion on the fatigue properties of

B. Obert, K. Ngo, J. Hashemi, and S. Ekwaro-Osire, Department of Mechanical Engineering, Texas Tech University, Lubbock, TX 79409; and **T. P. Sivam**, Flight Sciences Department, Raytheon Systems Company, Waco, TX 76715.

Nomenclature

l	length of area exposed to corrosion
t	thickness of sample
t_{calc}	calculated thickness of sample in corrosion area
w	width of exposed area
ρ	density of specimen material
A_{ex}	surface area of material exposed to corrosion
A_o	original cross-sectional area of gauge section
A_{ef}	effective cross-sectional area of gauge section assuming uniform corrosion, therefore uniform reduction in thickness
M_L	mass loss per unit area
ΔM	difference in mass before and after corrosion process (mass loss)
M_O	original mass of specimen

aircraft materials. The influence of corrosion on the fatigue life is central to the issues of aging aircraft. In studying the impact of corrosion on the fatigue properties of 7075-T6 aluminum alloy, Du *et al.*[6] demonstrated the extent of synergistic activity between corrosion and fatigue effects. In their study, the authors used the surface roughness as a revealing parameter in corrosion-fatigue interaction. Ma and Hoeppner[12] addressed the issues pertaining to pitting formation and shape as it relates to crack nucleation. In 1998, Fisher *et al.*[8] extended the understanding of the impact corrosion has on crack development and fatigue life of structures. The function of the corrosion phenomena on the integrity of structural elements was outlined.

Among aircraft aluminum alloys, 7075-T6 is widely used due to its comparatively high strength per unit weight and high fracture toughness. However, due to its composition, this aluminum alloy is susceptible to corrosion. There have been several studies on the corrosion and corrosion fatigue of aircraft aluminum alloys. Chen *et al.*[4] presented an overview of such a comprehensive program. The authors presented tools that could be applied in formulating approaches for service life prediction. Recently, Lin and Yang[11] carried out a study of the corrosion fatigue characteristics of 7050 aluminum alloy at various tempers. The authors demonstrated that higher tempers depicted a higher corrosion-fatigue-cracking resistance and stress-corrosion-cracking resistance. There is need to quantify the effects of corrosion on the static strength and fatigue life of 7075-T6 aluminum alloy. Of particular interest are the effects of pitting corrosion on the mechanical properties of the material. The quantification of mass loss per unit area, due to pitting corrosion, as a function of static strength and fatigue life could be a useful measure in the maintenance of aging aircraft.

The objective of this study was to quantify the effects of corrosion on the residual static strength and fatigue life of 7075-T6 aluminum alloy.[13] In accomplishing the objectives of the research, the test specimens were manufactured from the actual sheet material used in aircraft structures. This allowed for a more practical interpretation of results. In contrast to existing corrosion-related research in which paint-based masking is used, this research used a tape masking. Test specimens were corroded, in a confined area, using a galvanic corrosion cell. At different levels of corrosion, the mechanical properties of the specimens were extracted. In this paper, the experimental procedure and the corresponding tensile, fatigue, and hardness test data related to specimens of various material loss levels will be presented.

2. Accelerated Corrosion Procedure

The material used in this study was 1.6 mm (0.063 in.) thick sheets of 7075-T6 (bare) aluminum alloy. The chemical composition (wt.%) of the major elements in the studied alloy was 5.6Zn, 2.5Mg, 1.6Cu, 0.23Cr, and Al (balance). This alloy had a density of 2.80 g/cm^3 (0.10 lb/in^3) (Boyer and Gall[3]). The sheet material had the same thickness as the sheet metals used in the body structure of aircraft. This allowed for corrosion-affected tensile and fatigue results to be directly applicable to aging aircraft problems.

Test specimens of dimensions 304.8 mm (12 in.) in length and 76.2 mm (3 in.) in width were sheared from 304.8 × 609.6 mm (12 × 24 in.) plates delivered by the supplier. The specimens were cut such that when loaded, the loading axis would be perpendicular to the preferred grain direction. Each specimen was machined to a dog-bone shape with a centrally located gauge section of 63.5 mm (2.5 in.) in length and 50.8 mm (2 in.) in width, as shown in Fig. 1.

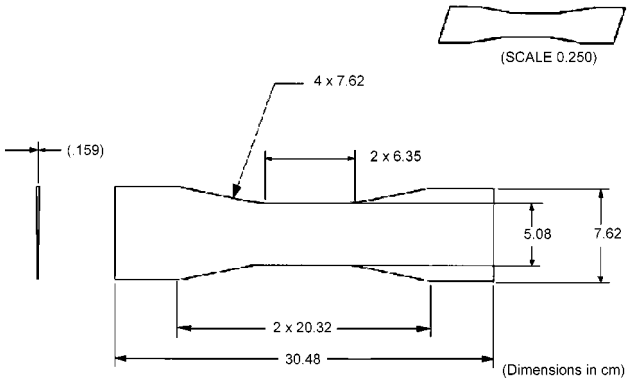

Fig. 1 Test specimen dimensions

In this study, only a small area on one side of the specimens at the center of the gauge section was corroded. Therefore, it was necessary for the remainder of the specimen to be protected from the corrosive environment by means of masking. Unlike existing research efforts where a corrosion-resistant paint or polymer coating was used, this research used a corrosion-resistant tape (a product of 3M (St. Paul, MN)) as the masking material. The corrosion resistant tape was applied to the specimen such that a section 45.7 × 63.5 mm (1.8 × 2.5 in.) was exposed on one side of the specimen. The exposed section was positioned in the center of the gauge section, as seen in Figure 2. The advantage of using tape was that after corrosion, no paint or coating removal process was required; the tape was simply peeled off. This eliminated unwanted mass loss due to chemical removal of masking material.

Corrosion of the samples was accomplished by the utilization of a corrosion cell. ASTM G 31-72[2] was referenced. The corrosion cell consisted of 71.9 L (19 gallon) plastic containers, salt water, power supply, anode, and cathode. The corrosion cell is shown in Fig. 3. The aluminum samples were used as the anode, graphite rods as the cathode, and salt water as the electrolyte to complete the cell. The salt water was produced by mixing Instant Ocean (Canton, MA) aquarium salt with distilled water. Approximately 100 g (1/2 cup) of salt was added to each 3.8 L (1 gal) of water, which resulted in water that closely simulated seawater. The specific gravity of the salt water was measured for each experiment and was found to be between 1.023 and 1.026, which correlates closely with natural seawater. The masked specimens were submerged in the salt water vertically and connected to the positive lead of the power supply. Next, the graphite rods were submerged and connected to the negative lead. The power supply was used to provide an induced voltage to the cell varying from 750 to 850 mV. The samples were then allowed to corrode to the desired material loss level in the corrosion cell. Previously, several test samples were corroded over various time intervals and their material loss was recorded. Using the recorded data, the material loss rate was

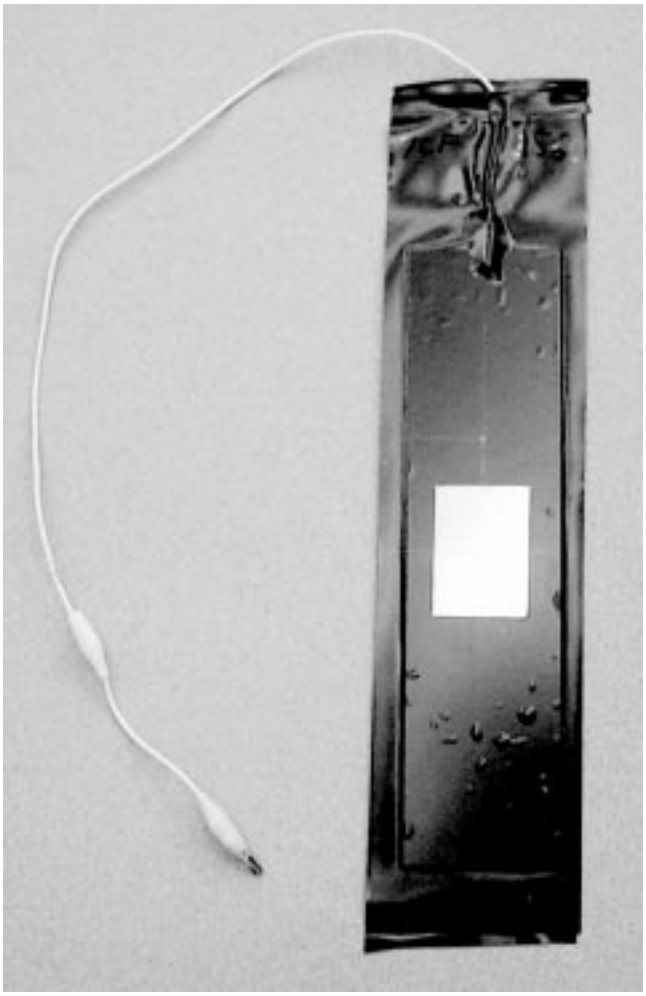

Fig. 2 Masked specimen showing exposed area to be corroded

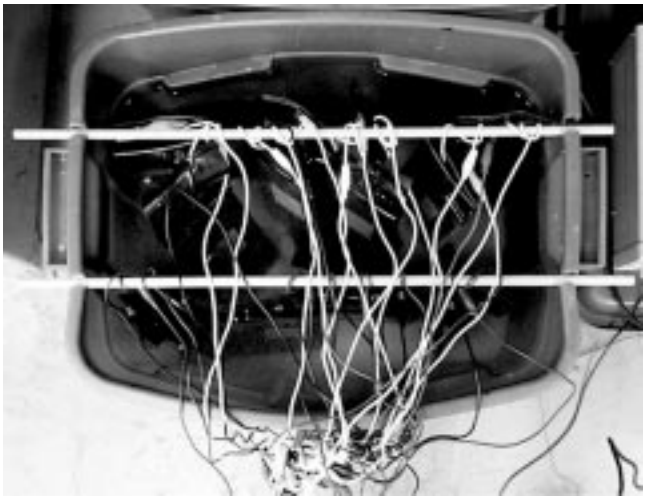

(**a**)

(**b**)

Fig. 3 The corrosion cell: (a) top view and (b) front view

calculated. The corresponding mass loss measurements versus the product of current and time are presented in Fig. 4. This information was used to predict when to remove the actual samples to achieve the desired mass loss groups.

After removing the specimens from the corrosion cell, they were unmasked and cleaned using a plastic bristle scrub brush to remove loose corrosion products. A visual examination of the corroded surface together with metalographical analysis of samples showed that general corrosion, pitting, and exfoliation were simultaneously at work, as seen in Fig. 5.

Another observation was that the corrosion seemed to be more intense at the edges of the corroded area next to the mask, as shown in Fig. 5. This crevice corrosion effect was not severe at low mass loss per unit area levels under 0.0672 g/cm^2 but became more significant at higher mass loss levels. Next, the specimens were cleaned using nitric acid (HNO_3) according to ASTM G 1-90.[1] After cleaning, the specimens were dried using a hair dryer and then weighed. The weight of the specimens was recorded before and after the corrosion process to determine the difference in mass. The mass loss per unit area, M_L, was calculated as a function of the difference in mass, ΔM, and the area of exposed aluminum, A_{ex}, as shown in Eq 1.

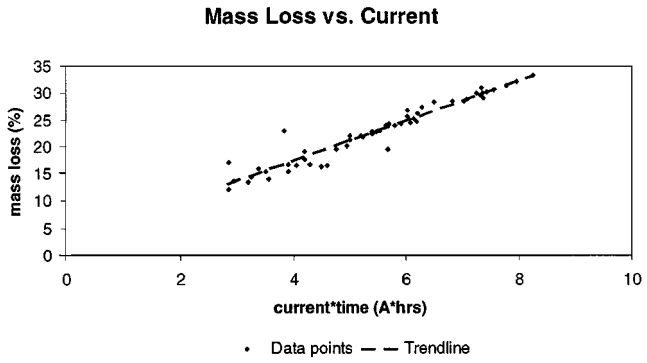

Fig. 4 Mass loss per area vs current * time

$$M_L = \frac{\Delta M}{A_{ex}} \qquad \text{(Eq 1)}$$

A total of 98 test specimens were prepared, according to gauge dimensions reported earlier, as seen in Fig. 6. The dimensions of the specimen and the corrosion area allowed for 2.54

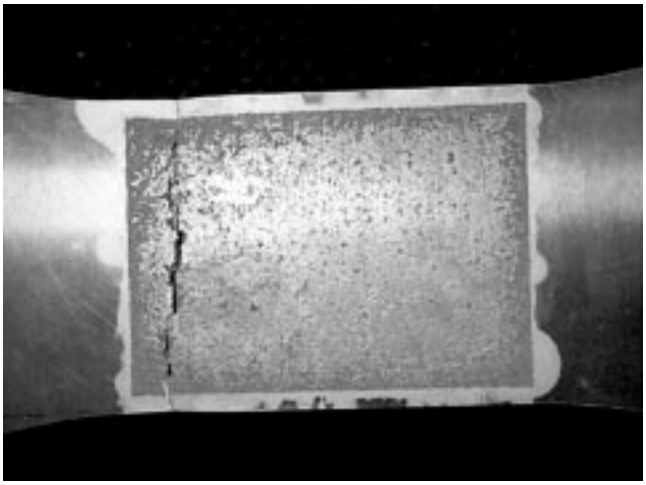

Fig. 5 Close-up of corroded area

mm (0.1 in.) of non-corroded material on both sides of the corroded area, as shown in Fig. 5 and 6. This feature assured that fatigue failures originated from the corroded area, and the results were not biased by edge effects.

3. Tensile, Fatigue, and Hardness Tests

The specimens were separated into seven groups, each consisting of 14 specimens. Based on Eq 1, the seven groups of specimens were corroded to target material loss levels of 0.0, 0.0224, 0.0448, 0.0672, 0.0896, 0.1120, and 0.1344 g/cm^2, respectively. The samples were corroded as accurately as possible, using the results shown in Fig. 4, to predict mass loss. In each group, half of the samples were used for tensile tests and the remaining half for fatigue tests. After corrosion, the surface of the specimen presented a uniformly pitted area with more corrosive action around the edges of the exposed area.

In this study, a servo-hydraulic material testing machine was used for fatigue and tensile tests. For signal control and data acquisition, Wavemaker-Runtime (Ver. 5.1) software was used. For static tensile testing, the rate of displacement used was 1 mm per min. The strain was acquired by means of an Instron (Canton, MA) extensometer attached to the gauge section of the specimen during testing. Tensile tests were performed on seven specimens of each material loss group. The tests were carried out to failure to determine the UTS. The UTS was calculated using both the original cross-sectional area of the gauge section, A_o, and an effective area, A_{ef}, assuming uniform corrosion and therefore uniform reduction in thickness of the cross-sectional area. The load used in determining the UTS was the maximum load recorded by the control software. An example of the effective cross-sectional area can be seen in Fig. 7. Equation 2 was used to calculate the effective area.

$$A_{ef} = (0.2^{*}t) + (M_o - \Delta M)/(l^{*}\rho) \qquad \text{(Eq 2)}$$

The fatigue samples were tested using the same machine and control software as the tensile test. The fatigue tests were conducted at a frequency of 10 Hz with a range in load varying

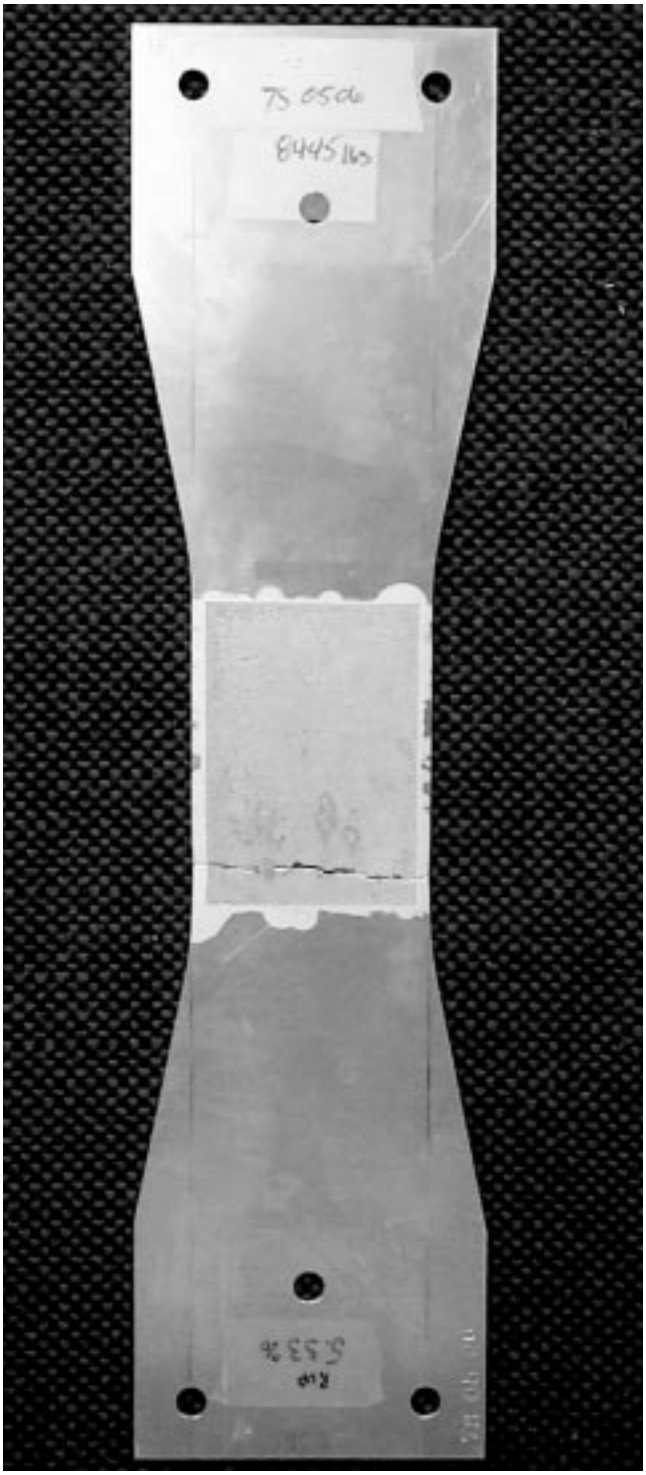

Fig. 6 Corroded specimen machined to dog-bone dimensions

from 8896 N (2000 lbf) to 889.6 N (200 lbf), corresponding to a stress ratio of 0.1. The load was applied first to the mean force level of 4893 N (1100 lbf) as a ramp function; then a sine wave function was applied with an amplitude of ±4003 N (± 900 lbf), resulting in the desired range of 8896 N (2000 lbf) to 889.6 N (200 lbf). Fatigue tests were first conducted

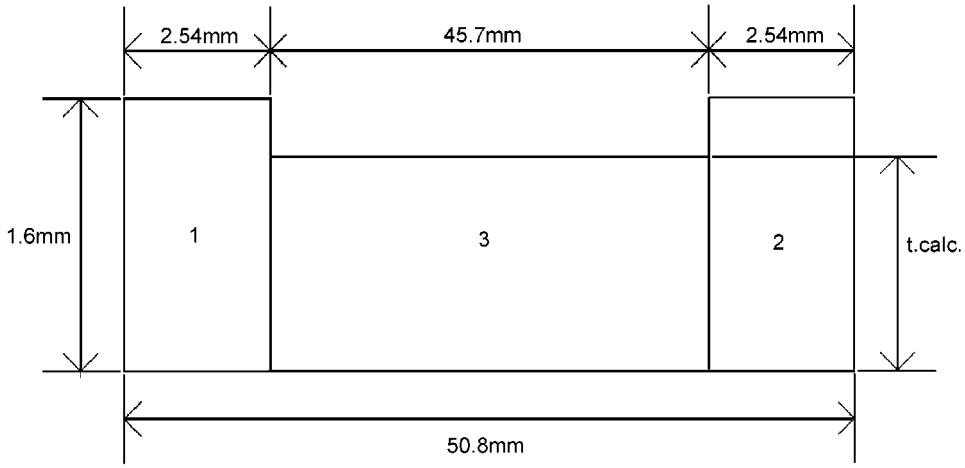

Fig. 7 Effective cross-sectional area assuming uniform corrosion, therefore uniform reduction in thickness

on seven un-corroded (M_L = 0.0 g/cm^2) specimens. These specimens were tested to a minimum of 3 million cycles. The samples were stopped soon after reaching 3 million cycles and not tested to failure due to time constraints. Fatigue tests were then performed on seven specimens within each mass loss per unit area group (0.0224, 0.0448, 0.0672, 0.0896, 0.1120, and 0.1344 g/cm^2). The fatigue tests conducted on corroded specimens were carried to failure to determine the reduction in fatigue life.

In addition to tensile and fatigue tests, Rockwell hardness tests were performed to measure the hardness of all specimens. A Wilson Rockwell Hardness tester was used to measure the hardness of each specimen at ten different points in the corrosion area. These points were selected in areas that showed no visible surface corrosion damage so that hardness could be accurately measured. The purpose of this exercise was to determine the effects of corrosion on hardness measurements.

4. Results and Discussion

The tensile test results of samples tested at different mass loss per unit area levels due to corrosion are shown in Fig. 8. As seen in this figure, there is a large initial drop in strength from the undamaged specimens to the 0.0224 g/cm^2 mass loss samples. For example, the difference in mean strength between the non-corroded and 0.0224 g/cm^2 mass loss samples is approximately 138 MPa (20 Kpsi); and the difference between the 0.0224 and 0.0448 g/cm^2 mass loss samples is approximately 27.6 MPa (4 Kpsi). After the 0.0224 g/cm^2 mass loss, the strength of the aluminum tends to reduce linearly with increasing mass loss per unit area. The mean value for mass loss per unit area and ultimate strength at each level is presented in Table 1.

The tensile test specimens tended to fail along the edge of the corroded area, as seen in Fig. 5. This could be attributed to the more severe pitting, hence the smaller cross-sectional area, observed at the edge of the corroded area. This effect is more evident at higher mass losses, which may be due to the increased exposure time required during corrosion.

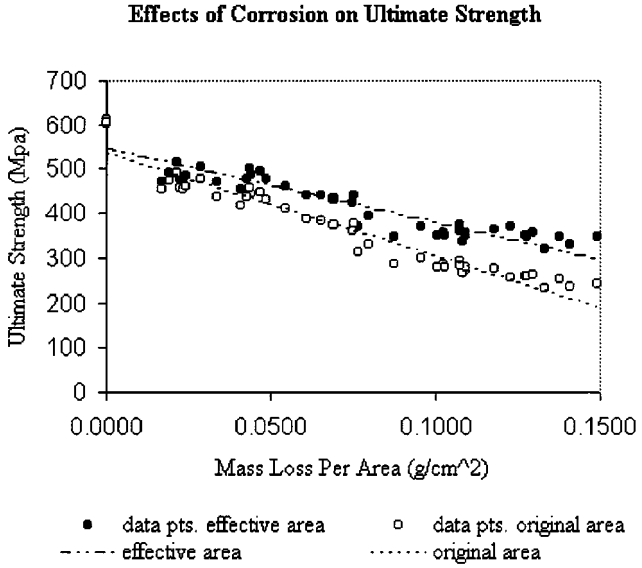

Fig. 8 Tensile strength vs mass loss per area

Table 1 Tensile test summary

Target value (g/cm^2)	Mass loss/area (g/cm^2)		Experimental UTS (original area) (MPa)		Experimental UTS (effective area) (MPa)	
	Mean value	Standard deviation	Mean value	Standard deviation	Mean value	Standard deviation
0.0000	0.0000	0.0000	606.1	4.83	606.1	4.8
0.0224	0.0222	0.0038	467.1	14.2	488.9	16.0
0.0448	0.0429	0.0048	439.2	12.7	480.6	15.8
0.0672	0.0669	0.0074	308.3	15.8	439.4	11.6
0.0896	0.0920	0.0109	295.8	19.2	362.6	16.0
0.1120	0.1116	0.0061	275.1	11.9	359.0	12.2
0.1344	0.1350	0.0080	249.2	11.9	342.1	13.3

Table 2 Fatigue test summary

Target value (g/cm^2)	Mass loss/area (g/cm^2)		Fatigue life (cycles)	
	Mean value	Standard deviation	Mean value	Standard deviation
0.0000	0.0000	0.0000	3,000,801*	. . .
0.0224	0.0246	0.0033	58,904	20,162
0.0448	0.0471	0.0050	47,682	17,553
0.0672	0.0689	0.0060	12,685	7343
0.0896	0.0946	0.0066	6835	3731
0.1120	0.1116	0.0053	4148	1123
0.0134	0.1350	0.0052	3802	906

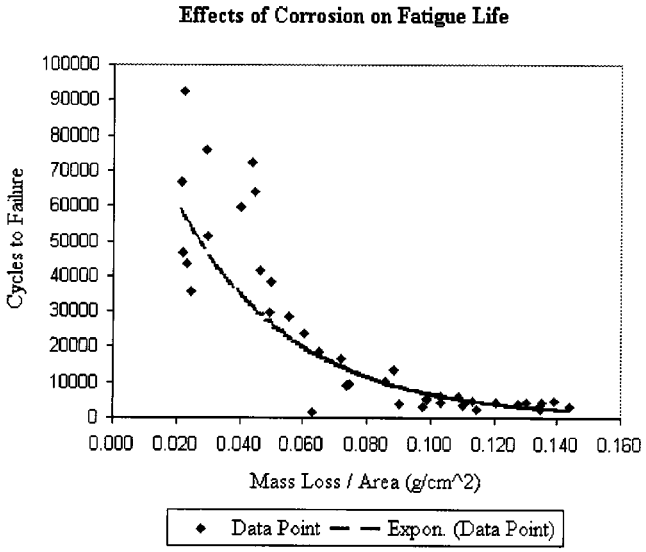

Fig. 9 Fatigue life vs mass loss per area

(**a**)

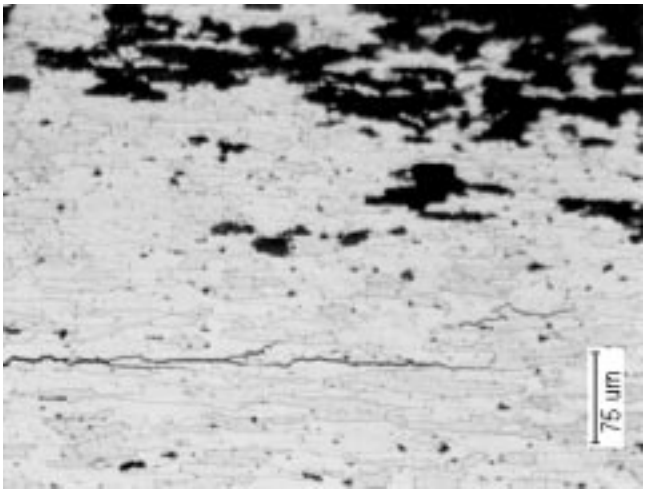

(**b**)

Fig. 10 Microstructure of corrosion samples: (a) cut along X- axis and (b) cut along Y-axis

Table 2 shows the mean value of mass loss per unit area and fatigue life for each level of corrosion. The results of the fatigue test conducted on samples of different mass loss levels are shown in Fig. 9. As seen in Fig. 9, the effect of corrosion tends to follow an inverse exponential trend. More specifically, the difference in average cycles to failure from 0.0224 to 0.0672 g/cm^2 is approximately 46,000 cycles, whereas the difference in average cycles to failure from 0.0896 to 0.1344 g/cm^2 is approximately 3000 cycles. Small amounts of corrosion reduce the life of the aluminum drastically. For example, the average life of samples tested with 0.0224 g/cm^2 mass loss per unit area was 58,904 cycles compared to the undamaged samples, which lasted 3 million cycles. This is a significant reduction in fatigue life even though the undamaged specimens were stopped soon after 3 million cycles and not tested to failure. This reduction in fatigue life is due to stress concentrations created by subsurface damage formed in the specimen as a result of corrosion.

In order to investigate the subsurface damage, corroded specimens were prepared for metallurgical examination. Sections to be viewed were cut from the corroded area of untested samples. One section was cut along the *X*- (horizontal) axis and one along the *Y*- (vertical) axis, as indicated in Fig. 5 and 6. This was done to get a better picture of the pit topology. The samples were then mounted in a polymer resin such that the thickness could be viewed. Next, the samples were sanded and polished to a .1 μm finish. The samples were etched using Keller's reagent (2 mL 48% HF, 3 mL HCL, 5 mL HNO_3, 190 mL H_2O). The samples were then viewed using a metallograph, and photos were made of the samples for comparison and analysis. The resulting images are shown in Fig. 10 (a) and (b). These figures show that the corrosion penetrates into the thickness of the metal deeper than can be seen at the surface. It is due to the existence of this subsurface corrosion that the reduction in hardness occurs. The section cut from the Y- axis shows an internal crack believed to be induced by corrosion in combination with residual stresses present in the test material. A detailed examination of the crack shows that it is running along the grain boundaries and not across them. This observation indicates that this crack is corrosion induced. Next, a section was cut from a specimen that failed in fatigue. The sample was

cut so that the length of the fracture surface could be viewed. The sample was prepared in the same manner as described previously. The resulting image can be seen in Fig. 11. A fatigue induced crack such as the one in Fig. 11 runs across the grains and looks very different than the crack seen in Fig. 10 (b).

Another trend, observed from the fatigue tests, was that fracture initiated at deep pits and, after a few cycles, propagated across the width of the specimen. In order to investigate the effect of pit depth, the minimum thickness of the specimens was measured using vernier calipers at the thinnest area of the fracture surface. The thickness of the specimen was also calculated by estimating uniform reduction in thickness of the corroded area, as seen in Fig. 7. The thickness was calculated using Eq 3:

$$t_{\text{calc.}} = \frac{M_o - \Delta M}{\rho^* l^* w} \qquad \text{(Eq 3)}$$

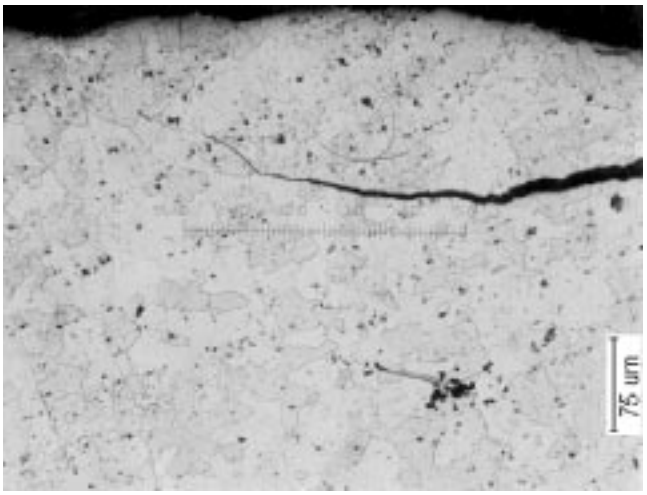

Fig. 11 Microstructure of fracture surface

A plot was made of the cycles to failure versus measured thickness and versus calculated thickness; the results are shown in Fig. 12. Here it is assumed that the minimum thickness at the fracture surface represents the pit depth at which fracture started.

The hardness of each specimen was measured at ten different points in the corrosion area. The hardness was measured on the Rockwell B scale and converted to the Brinell scale using a New Age Industries conversion table (ASTM 18 and E140 reprinted with permission) For the noncorroded specimens, the average hardness value was found to be 92 HRB (163 HB). For the specimens in the 0.0224 g/cm^2 mass loss per unit area group, the average hardness value dropped to 66 HRB (104 HB). The drop in the hardness is due to sub-surface material loss, which is not detectable with the naked eye. The average hardness values for 0.0448 and 0.0672 g/cm^2 mass loss groups were 65 HRB (102 HB) and 61 HRB (96 HB), respectively. For mass loss levels above 0.0672 g/cm^2, the hardness measurements were not reliable because of the flaky nature of the surface of the material due to exfoliation.

5. Conclusions

It was observed that the fatigue life tends to follow an inverse exponential reduction in life as mass loss per unit area increases. The reduction in fatigue life is due to stress concentrations as a result of pit formation and subsurface corrosion. After corrosion was initiated, there appeared to be a linear decrease in strength with increasing material loss. The severe drop in both static strength and fatigue life of the corroded specimens does not correlate well with pit depth or mass loss per unit area. For example, even the slightest mass loss per unit area results in a large drop in fatigue life and UTS. The reason for the drastic drop in static strength and fatigue life of the specimens is due to pit geometry and the interaction of pits with one another.

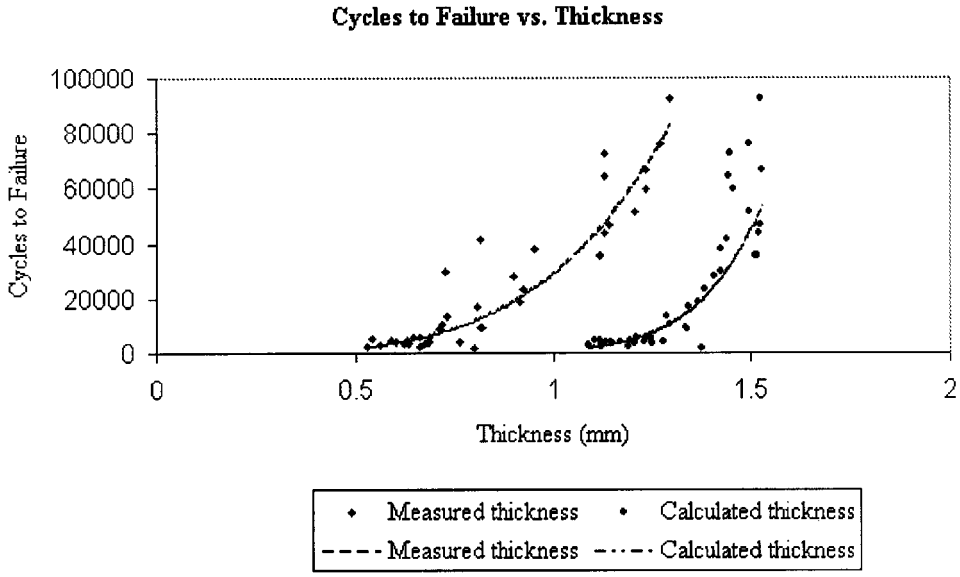

Fig. 12 Fatigue life vs minimum thickness curves

Acknowledgments

The authors gratefully acknowledge Mr. Barry Eaton, Manager, and Mr. Richard Ely, Senior Staff Specialist Engineer, Flight Sciences Department, Raytheon Systems Company, for their interest and support of this research program.

References

1. *Standard Practice for Preparing Cleaning, and Evaluating Corrosion Test Specimens*, ASTM G 1-90 Standard, ASTM, Philadelphia, PA, 1994.
2. *Standard Practice for Laboratory Immersion Corrosion Testing of Metals*, ASTM G 31-72 Standard, ASTM, Philadelphia, PA, 1994.
3. H.E. Boyer and T.L. Gall: *Metals Handbook*, ASM, Metals Park, OH, 1985.
4. G.S. Chen, M. Gao, D.G. Harlow, and R.P. Wei: "*Corrosion and Corrosion Fatigue of Airframe Aluminum Alloys*," NASA Conference Publication No. 3274//P1, NASA, Washington, DC, 1994, pp. 157-73.
5. V.R. Crispim and J.J.G. da Silva: *Appl. Rad. Isotopes*, 1998, vol. 49(7) pp. 779-82.
6. M.L. Du, F.P. Chiang, S.V. Kagwade, and C.R. Clayton: *J. Testing Eval.*, 1998, vol. 26(3), pp. 260-68.
7. A.A. Feinberg, G.J. Gibson, J.V, White, and R.E. Briggs: *Proc. Inst. Environ. Sci.*, 1994, vol. 40, pp. 198-210.
8. J.W. Fisher, E. Kaufmann, and A.W. Pense: *Transportation Research Record* No. 1624, 1998, pp. 110-17.
9. G.S. Frankel: *J. Electrochem. Soc.*, 1998, vol. 145(6), pp. 2186-98.
10. R.E. Green: "*Emerging Technologies for NDE of Aging Aircraft Structures*," Materials Research Society Symposia Proceedings, Materials Research Society, Pittsburgh, PA, 1998, vol. 503, pp. 3-14.
11. C.-K. Lin and S.-T. Yang: *Eng. Fract. Mech.*, 1998, vol. 59(6), pp. 779-95.
12. L. Ma and W. Hoeppner: "*The Effects of Pitting on Fatigue Crack Nucleation in 7075-T6 Aluminum Alloy*," NASA Conference Publication No. 3274//P1, NASA, Washington, DC, 1994, pp. 425-440.
13. B. Obert, K. Ngo, J. Hashemi, S. Ekwaro-Osire, and T.P. Sivam: ''Quantification of Corrosion in 7075-T6 Aluminum Alloy'' Recent Advances in Solids and Structures, 1999 ASME International Mechanical Engineering Congress and Exposition, 1999, PVP, vol. 398, pp. 119–33.